

# Light–matter interactions in quantum nanophotonic devices

Alejandro González-Tudela<sup>1</sup>✉, Andreas Reiserer<sup>2</sup>, Juan José García-Ripoll<sup>1</sup> & Francisco J. García-Vidal<sup>3,4</sup>✉

## Abstract

Nanophotonics offers opportunities for engineering and exploiting the quantum properties of light by integrating quantum emitters into nanostructures, and offering reliable paths to quantum technology applications such as sources of quantum light or new quantum simulators, among many others. In this Review, we discuss common nanophotonic platforms for studying light–matter interactions, explaining their strengths and experimental state-of-the-art. Each platform works at a different interaction regime: from standard cavity quantum electrodynamics (QED) setups to unique quantum nanophotonic devices, such as chiral and non-chiral waveguide QED experiments. When several quantum emitters are integrated into nanophotonic systems, collective interactions emerge, enabling miniaturized, versatile and fast-operating quantum devices. We conclude with a perspective on the near-term opportunities offered by nanophotonics in the context of quantum technologies.

## Sections

Introduction

Light and matter in quantum nanophotonics

Individual emitter phenomena

Collective effects

Outlook

<sup>1</sup>Institute of Fundamental Physics IFF-CSIC, Madrid, Spain. <sup>2</sup>Technical University of Munich, TUM School of Natural Sciences and Munich Center for Quantum Science and Technology (MCQST), Garching, Germany. <sup>3</sup>Departamento de Física Teórica de la Materia Condensada and Condensed Matter Physics Center (IFIMAC), Universidad Autónoma de Madrid, Madrid, Spain. <sup>4</sup>Institute of High Performance Computing, Agency for Science, Technology, and Research (A\*STAR), Singapore, Singapore. ✉e-mail: [a.gonzalez.tudela@csic.es](mailto:a.gonzalez.tudela@csic.es); [fj.garcia@uam.es](mailto:fj.garcia@uam.es)

## Key points

- Nanophotonics is the field that studies how to control the properties of light at the nanoscale.
- It began in the late 1980s with the discovery of photonic crystals, followed by subsequent waves that harnessed metals and metamaterials to engineer unique photon flows at the (semi)classical level.
- Current experimental efforts aim at integrating these setups with natural and artificial atoms to control the light properties at the quantum level.
- Apart from reducing the mode volume of light and thus enhancing light–matter interactions, nanophotonic setups allow the exploration of new regimes that exploit non-trivial energy dispersions and polarization patterns.
- Quantum nanophotonics creates unique opportunities to develop a new generation of miniaturized, versatile and fast-operating quantum technologies.

## Introduction

In quantum technologies, light – and its interaction with matter – plays a pivotal role. At present, optical photons are the only viable candidate for long-distance quantum communication, thanks to their long coherence times<sup>1</sup>. These photons can protect the transmission of information against eavesdropping attacks by using quantum key distribution protocols<sup>2</sup> but also connect different quantum nodes for performing distributed quantum algorithms<sup>1</sup>. In the latter case, cavity quantum electrodynamics (QED)<sup>3</sup>, that is, the interaction between emitters and localized photonic modes, provides a link between propagating qubits encoded in the light and the stationary qubits encoded in the emitters. Beyond providing this link, the exchange of photons between emitters can also lead to photon-mediated interactions between them, which can be harnessed for building two-qubit entangling gates or, in a more passive role, for inducing optical trapping potentials to generate ordered atomic arrays that can serve as a basis of new analog quantum simulators<sup>4,5</sup>. Last but not least, the interaction of light and matter can induce strong interactions between light fields at the single-photon level. These interactions are instrumental in generating non-classical states of light with the potential to surpass classical metrological limits<sup>6</sup>, to create quantum-error-corrected bosonic codes<sup>7,8</sup> or to implement general-purpose measurement-based quantum computing<sup>9</sup>.

These applications demand efficient light–matter interfaces connecting seemingly disparate quantum objects: particles propagating at the fastest possible speed with no interactions (light) and stationary quantum systems interacting strongly at short distances (matter). Intuitively, efficiency means here that the probability that a single photon interacts with a single emitter must be significant. In free space, this probability depends on the ratio between the scattering cross-section of the emitter and the mode area of the light impinging on it. It is thus strongly limited by diffraction, which sets a minimum light confinement for a given wavelength. Diffraction also limits the probability that a photon created at one emitter is absorbed by another

at a different position, as light spreads in all directions. This diffraction makes the photon-mediated interactions induced by these processes decay rapidly with distance, precluding the observation of quantum cooperative phenomena. Several strategies have been pursued in the past 20 years to overcome these limitations. Some of them involve confining the emitters among highly reflecting mirrors to increase the number of times that a photon passes a single emitter<sup>10</sup>, placing more emitters in a given region to increase the probability that a photon interacts with at least one of them<sup>11</sup>, or using highly excited (Rydberg) atomic states to increase the emitters' dipole moments<sup>12</sup> and thus the light–matter interaction strength. However, in all these platforms, diffraction will ultimately dictate the strength and spatial nature of the interactions.

Over the past 15 years, an alternative approach has emerged that can overcome these limitations: quantum nanophotonics<sup>13,14</sup>. The idea is to interface emitters with photons, or photon-like excitations, confined in subwavelength-engineered materials such as dielectrics or metals. Unlike free space, nanophotonic devices can confine photons on subwavelength scales. This enables device miniaturization, stronger light–matter interactions and, consequently, faster dynamics and operation speed of the resulting quantum technologies. Moreover, this confinement allows for qualitatively different light–matter interaction regimes, such as chiral ones<sup>15</sup>, thanks to the longitudinal component of the electric field when confined to subwavelength scales. Beyond single-emitter phenomena, the propagation of photons in 1D or 2D geometries also enhances the probability that the photons created by one emitter are absorbed by a different one, enabling long-range photon-mediated interactions between emitters and their application to create entanglement<sup>16,17</sup>. Finally, a suitable design of the photonic metamaterial enables both the engineering of photonic energy dispersion and the establishment of sophisticated connectivities between tunable emitters, with no analogue in other quantum optical setups, such as topologically protected models<sup>18</sup>. In summary, quantum nanophotonics provides faster and smaller light–matter interfaces and enables access to qualitatively new physics.

In this Review, we discuss the theory, state-of-the-art and future applications of such quantum nanophotonic devices. As a complement to earlier reviews covering quantum dots<sup>13</sup>, atomic systems<sup>14</sup>, waveguide QED<sup>19</sup>, quantum plasmonics<sup>20</sup> or chiral photonic devices<sup>15</sup>, our goal is to provide a broad and high-level perspective of all nanophotonic platforms. We thus begin by introducing the various candidates for matter and light degrees of freedom, discussing the state-of-the-art nanophotonic light–matter interfaces that they enable. We then explain the variety of phenomena in the single- and many-emitter scenarios, both in confined cavity QED and open waveguide QED environments. Here, we cover work from the semiclassical Purcell regime, as in other existing reviews<sup>21</sup>, to the purely quantum nonlinear behaviour. We conclude with a selection of experimental challenges and opportunities for quantum nanophotonics in the near term.

## Light and matter in quantum nanophotonics

The term ‘light–matter interface’ describes a plethora of physical systems combining a finite number of emitters (the matter part) each with (at least) an optical transition that interacts with discrete or continuous photonic degrees of freedom. In what follows, we review the state-of-the-art quantum nanophotonic platforms and explain the advantages and disadvantages of the different types of emitters and photonic degrees of freedom considered.

## Matter

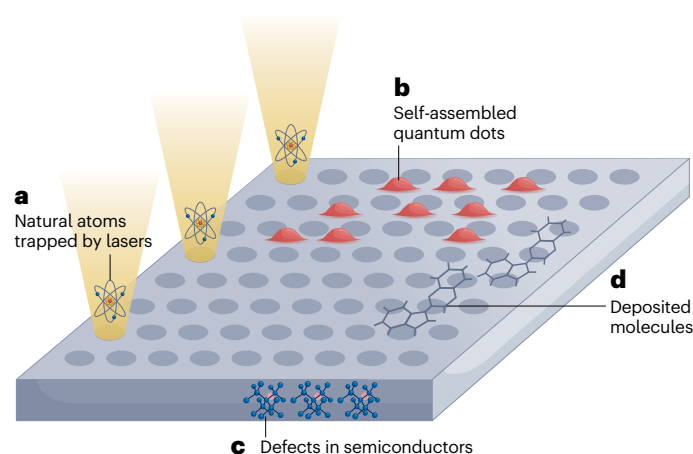
Several types of emitters can be coupled to nanophotonic structures (Fig. 1). These include quantum dots<sup>13</sup>, defect centres in semiconductors<sup>22–27</sup>, excitons in 2D materials<sup>28,29</sup>, individual molecules in a crystalline host<sup>30</sup>, as well as atoms trapped in vacuum<sup>31–35</sup>. For all of these coupled emitters, the interaction with light is described either through the polarizability of the emitter in semiclassical descriptions, or through its dipole transition matrix element in fully quantum mechanical treatments. The larger the polarizability or dipole matrix element, the stronger the light–matter interaction. Typically, each emitter hosts an optically active electronic excitation such that the tighter the potential that confines the electron, the lower the polarizability or dipole element, and the weaker the light–matter interaction. Quantum dots are the fastest emitters because the electron is loosely confined by a semiconductor band structure<sup>13</sup> that enables typical radiative decay rates on a subnanosecond timescale. Molecules<sup>30</sup>, atoms<sup>36</sup>, and defects in semiconductors<sup>23,24,26</sup> exhibit a typical emission in the range of a few nanoseconds when considering dipole-allowed transitions. Other emitters with first-order forbidden transitions decay much more slowly. Such is the case for rare-earth dopants, where the electron is in an inner 4*f*-shell tightly confined to the nucleus, leading to decay rates from 0.2 ms (ref. 25) up to tens of milliseconds<sup>27</sup>. However, the decay rate is only one of the many figures of merit to consider when integrating emitters into nanophotonic structures. Other equally important concerns are how to place the emitters in (or by) the nanostructures, how to keep the coherence of the emitters and their interaction with light, the spectral homogeneity of the emission, and the possibility of having multiple field-coupled ground states to enable quantum memories or to engineer Raman-assisted transitions.

Cold atoms<sup>31–35</sup> can achieve excellent coherence and spectral homogeneities. Besides this, they typically exhibit several hyperfine ground states where quantum information can be stored. However, when integrating them with nanophotonic structures, one faces the experimental overhead of trapping the atoms near the nanostructures and cooling them to their ground state. Trapping is challenging because decreasing the distance to the material enhances the surface-induced noise and the van der Waals forces that attract the atoms to the surface. To prevent both problems, trapping potentials are generally deeper than free-space optical potentials, which implies using larger laser intensities. This is why experiments should involve nanophotonic materials with low absorption, such as glass<sup>31</sup> or silicon nitride<sup>32,33</sup>. Typical trapping configurations use two-colour traps via guided modes of optical nanofibres<sup>31,35,37–40</sup> and photonic-crystal waveguides<sup>32,41,42</sup>. This is a very robust approach that has reliably trapped thousands of atoms near optical fibres<sup>31,37</sup>. The main drawbacks are that the trapping occurs far from the surface, which limits the emitter–photon interaction strength, and that the process is still probabilistic (only has a certain probability of success). Optical tweezers are a promising alternative to improve loading efficiency, for example by using Laguerre–Gauss beams<sup>13</sup>. In this setup, the interference of a laser beam with its reflection from the nanostructure creates a deep trap close to the surface<sup>33,44–46</sup>. The main advantage of using optical tweezers is the potential to scale up to large and deterministic atom numbers with the methods developed for free-space traps<sup>47–49</sup>. However, work still needs to be done on how to integrate these methods near nanophotonic structures so that the atoms can be trapped close to the structure<sup>46,50,51</sup>.

The trapping challenges of cold atom systems are avoided with other emitters, such as self-assembled quantum dots<sup>13</sup>, molecules in dielectric matrices<sup>30</sup>, or defect centres in semiconductors<sup>23,24,26</sup>.

In all these cases, the trapping occurs by embedding the emitter in a crystal, and the cooling is done by a refrigerator. The price to pay, however, is an often noisier environment and the spectral inhomogeneities arising from imperfect fabrications and charge fluctuations. The choice of the emitter and host is crucial to avoid decoherence induced by the environment. For example, emitters with a spin degree of freedom that can implement long-lived quantum memories are better integrated into crystals containing no other magnetic moments. Moreover, the decoherence induced by phonons radically decreases on working at cryogenic temperatures ranging from a few millikelvin<sup>52,53</sup> up to a few kelvin temperatures<sup>13,23–25,30</sup>, depending on the host and emitter. Currently, the leading candidates are silicon, diamond and silicon carbide<sup>54</sup>, all of which are transparent at the wavelength of interest and offer a high refractive index enabling the tight confinement of light fields in nanostructures.

Spectral inhomogeneities are the main challenge to observing quantum effects with solid-state emitters, even when the structure-induced decoherence is under control. Local controls, by electrical fields or other means, can often correct static spectral inhomogeneities arising, for example, from local strain in defect centres and molecules, or size fluctuations in quantum dots. However, dynamical frequency fluctuations – known as dephasing or spectral diffusion when the timescale is faster or slower than a radiative lifetime, respectively – are much harder to correct. This decoherence originates in magnetic and electric field fluctuations – ‘spin’ or ‘charge noise’, respectively. To minimize these fluctuations, one can aim for purer crystals without



**Fig. 1 | Schematic representation of emitters integrated with a nanophotonic structure (not to scale).**

**a**, Individual atoms can be trapped by laser light in the structure’s proximity. Despite the technical overhead, this setup avoids cryostats and supports emitters with a very small spectral inhomogeneity and spin states with long coherence, for example hyperfine clock states. **b**, Quantum dots can be generated by growing islands of semiconductors with a different bandgap within the structure. They show fast radiative emission but large spectral inhomogeneity because of unavoidable size fluctuations and spectral diffusion caused by charge noise. The Overhauser field typically also limits spin coherence. **c**, Optically active dopants and colour centres can be included in the nanostructure during growth or by implantation. Their spectral and spin coherence properties strongly depend on the host and emitter. Good spectral stability can be obtained for inversion-symmetric emitters, and very long coherence can be obtained using nuclear spins. **d**, Individual molecules can be deposited individually or in thin films onto the nanostructure. Although they are chemically identical, their unavoidable proximity to interfaces typically leads to inhomogeneity and spectral diffusion.

paramagnetic impurities and charge traps, try to freeze magnetic impurities and charge traps with strong magnetic or electric fields, and keep the emitters separated from interfaces. These strategies have led to considerable progress in the stability of the quantum emitters' transitions in recent decades. Quantum dots were the first to demonstrate radiatively limited coherence<sup>55</sup>, and their main challenge is to avoid the Overhauser field that spoils the coherence of their memory levels (although it can reach 0.1 ms under dynamical decoupling<sup>56</sup>). Molecules can also exhibit coherence in nanowaveguides<sup>57</sup> and cavities<sup>58</sup>, but so far lack long-term memory<sup>30</sup>. Defect centres, in contrast, have demonstrated long-lived memory combined with Fourier-limited emission and high-fidelity operations<sup>59,60</sup>. Recently, they also achieved single-emitter spectral diffusion linewidth as low as <0.2 MHz, close to an interface – albeit not radiatively limited – by using inversion-symmetric sites<sup>53</sup>.

## Light

The seminal 1932 paper introducing Fermi's golden rule<sup>61</sup> determined that an emitter's decay rate grows with the dipole matrix element and depends on both the emitter's properties and the available density of photonic states<sup>62</sup>. The latter can be controlled by modifying the environment around the emitter, using nanophotonic structures. Macroscopic Maxwell equations describe light propagation in these materials through the electrical permittivity  $\epsilon$  or refractive index  $n$ . The imaginary part of the permittivity determines the absorption of the material, while the real part controls the refraction. Together, they enable the confinement of light – the larger  $\epsilon$ , the tighter the possible confinement. In what follows, we summarize the main available nanophotonic structures in chronological order of discovery and describe their main pros and cons.

Historically, the first nanophotonic modes to be studied described photons confined within engineered dielectric materials and represented either localized photonic modes in defect photonic-crystal cavities<sup>33,63</sup> or propagating photons in 1D optical fibres<sup>31,35,37–40</sup> and photonic-crystal waveguides<sup>13,32,64,65</sup>. The great advantage of these setups is that dielectrics can be engineered to have low absorption in the optical regime, yielding high-quality factors for the localized modes and long propagation lengths for the propagating ones. The main drawback is that the subwavelength confinement is generally limited to the enhancement provided by the refractive index. However, recent work has shown that subwavelength material discontinuities<sup>66–68</sup>, which can be created in engineered dielectric cavities, support confined light modes at deep subwavelength scales of  $10^{-3}(\lambda)^3$  with high-quality factors  $Q \approx 10^3$ – $10^5$ .

The next wave in nanophotonics harnessed metallic systems, in the form of plasmonic cavities built from metallic nanoantennae and plasmonic waveguides. In these materials, the bulk electron oscillations from the metal hybridize with the electromagnetic excitations, forming surface plasmons that propagate along the metal–dielectric interface<sup>69,70</sup>. These structures confine light at deeply subwavelength scales<sup>71</sup>, sometimes reaching picometre mode sizes<sup>72</sup>, thus boosting single-photon coupling strengths. However, this confinement comes at the cost of severe absorption losses, yielding broad resonances with poor quality factors and short propagation lengths. Hybrid metal–dielectric cavities<sup>73–75</sup> embody a strategy to overcome these limitations, combining the deep subwavelength confinement of surface plasmons with the low loss of the dielectrics. Despite recent proof-of-principle realizations of this idea<sup>74,75</sup>, much work is needed to exploit this new platform's potential.

In addition, there are other avenues opened in nanophotonics that are complementary and synergistic with the previous ones. Metamaterials<sup>76</sup> are subwavelength-periodically modulated structures with exotic optical responses, such as negative refractive indices<sup>77,78</sup>. Metamaterials have often been studied in the classical regime to obtain perfect lensing or cloaking effects. However, there is a growing interest in using their properties also in the quantum regime, for tasks such as engineering strongly correlated photonic states<sup>79</sup> or obtaining non-trivial emitter interactions due to the unconventional energy dispersion of their excitations<sup>80,81</sup>. The great challenge of metamaterials lies in fabrication, especially in the optical regime, which requires the control of structures at the nanometre scale.

Finally, another direction is exporting topological concepts from condensed matter into photonics<sup>82</sup>. The study of topological effects is not limited to electronic systems and can also be explored using photons<sup>83</sup>. A photonic equivalent of the quantum Hall effect can be obtained using magneto-optical materials, which results in a bulk band with a non-trivial topological invariant and the emergence of chiral topological boundary modes propagating along the edge of the device. The photonic quantum Hall effect, which has been demonstrated in the microwave regime<sup>84</sup>, opened an exciting playground in which to realize unconventional photon flows, such as one-way and robust-to-disorder photon propagation, among other phenomena<sup>82</sup>. However, magneto-optical effects are weak in the optical regime, and the exploration of topological order requires different approaches based on symmetry-protected phases.

## Individual emitter phenomena

When a single emitter couples to the electromagnetic modes confined in photonic structures, there are a number of light–matter interaction regimes with different phenomenology. In general, the conservative part of the light–matter interaction Hamiltonian in quantum nanophotonic devices is well described by the Hamiltonian  $H_I = \sum_i (g_i a_i^\dagger \sigma + \text{H. c.})$  (Box 1). The dipole operator of the emitter  $\sigma$  appears with the bosonic annihilation  $a_i$  and creation  $a_i^\dagger$  operators for each photonic mode that couples to the optical transition of the emitter. Its coupling strength  $g_i$  is proportional to the scalar product of the transition dipole of the emitter and the electric field at the emitter's position, which is inversely proportional to the square root of the mode volume of the associated light mode. This Hamiltonian assumes the local-dipole and rotating wave approximations. The latter is generally valid in the optical regime (independent of the size of the emitter), while the former is violated only for small-scale devices<sup>85</sup> or large emitter sizes<sup>86</sup>. If additional decay channels are included, one must upgrade to a density matrix description, whose effects enter as Lindblad decay terms. Although the same model describes most situations of interest in nanophotonics, the nature of the photonic modes exposes qualitatively different physics. In what follows, we describe the different light–matter interaction regimes, from standard cavity QED for emitters in localized photonic modes to waveguide QED or chiral or topological light–matter interfaces enabled by nanophotonic devices.

### Cavity QED

Cavity QED names a regime in which a single two-level emitter with transition frequency  $\omega_{eg}$  interacts with a single localized photonic mode of frequency  $\omega_a$ . This regime appears in different nanophotonic setups, such as localized defects in 2D<sup>63</sup> and 1D<sup>33</sup> photonic-crystal waveguides, or in plasmonic<sup>71,72</sup> or hybrid plasmon–dielectric nanoantennas<sup>57</sup> (Table 1).

## Box 1

### Cavity versus waveguide quantum electrodynamics

Cavity quantum electrodynamics (QED) refers to the study of light–matter interaction between quantum emitters and a localized photonic mode. In its simplest instance, that is, when a two-level emitter couples to a single-cavity mode, their dynamics is described by the well-known Jaynes–Cummings model:

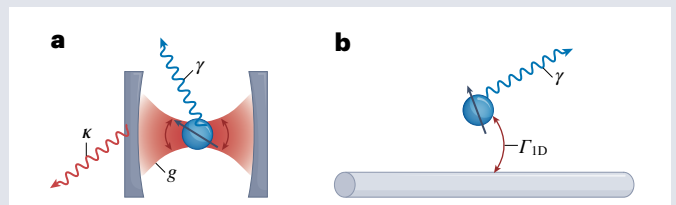
$$H = \omega_{eg} \sigma^\dagger \sigma + \omega_a a^\dagger a + g(a^\dagger \sigma + \sigma^\dagger a), \quad (1)$$

where  $\omega_{eg}$  and  $\omega_a$  represent the frequency of the optical transition of the emitter and cavity modes, respectively, and  $g$  is the coupling strength. The latter has to be compared with the cavity losses,  $\kappa$ , and the decay of the emitter into other channels,  $\gamma$ . When the coupling strength overcomes the losses,  $g > \kappa, \gamma$ , the system is said to be in the strong-coupling regime, in which the light–matter degrees of freedom form new quasiparticles called polaritons. This regime leads to nonlinear frequency shifts, which can be harnessed to induce photon blockade or for quantum non-demolition measurements. The opposite regime, that is,  $g < \kappa, \gamma$ , when the system is in the weak-coupling regime, leads to purely dissipative dynamics, and the cavity mostly renormalizes the lifetime of the emitter through the Purcell enhancement:  $\Gamma_{\text{cav}} = g^2/\kappa$ . An important parameter that characterizes both cavity QED regimes is the ‘cooperativity’ that measures the ratio between the emission into the cavity and into the other decay channels:

$$C = \frac{\Gamma_{\text{cav}}}{\gamma} = \frac{g^2}{\kappa\gamma}. \quad (2)$$

In this limit, the coherent dynamic simplifies to the well-known Jaynes–Cummings Hamiltonian<sup>88</sup>, where  $g$  is the coupling strength between the emitter and the cavity mode. This coherent exchange competes with the decoherence mechanisms, which, in addition to the solid-state decoherence sources introduced above, now also include the photon loss from the cavity modes and the emitter decay into other channels, denoted here by  $\kappa$  and  $\gamma$ , respectively. The competition between coherent and dissipative dynamics separates the weak- and strong-coupling cavity QED regimes.

The first experimental demonstrations of nanophotonics cavity QED operated in the weak-coupling regime. This was owing to the experimental challenges of achieving the strong-coupling regime, which requires building cavities with high-quality factors (large  $Q$ , low  $\kappa$ ) and deterministically positioning the emitters for a consistent, large interaction strength  $g$ . In the weak-coupling limit, the emitter experiences a mostly irreversible dynamics in which the cavity becomes an additional decay channel ( $\Gamma_{\text{cav}}$ ). The first experimental signature of this regime with quantum dots in photonic-crystal cavities<sup>89,90</sup> and with trapped atoms in photonic crystals<sup>33</sup> was precisely an enhanced spontaneous emission decay rate  $\Gamma_{\text{em}} = \gamma + \Gamma_{\text{cav}}$  measured through dynamical photoluminescence (Fig. 2a) or the complementary linewidth broadening in the spectrum (Fig. 2b). The weak-coupling regime may have various quantum technological applications when the decay into the cavity channel exceeds other channels – that is, when the cooperativity parameter is greater than 1



This Purcell regime is largely connected to the physics of waveguide QED, that is, the interaction of emitters with 1D propagating modes. In this system, the dynamics is generally irreversible, as the photons generally are not reabsorbed by the emitters. The lifetimes of the emitters are also renormalized by the presence of the waveguide, owing to the mode transversal confinement and potential reduction of the photon speed (slow light). The typical figure of merit that characterizes how well the emitters are coupled to the light mode is the  $\beta$ -factor defined by the ratio between the emission into the waveguide and into the rest of the channels:

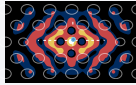

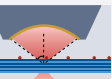

$$\beta = \frac{\Gamma_{1D}}{\Gamma_{1D} + \gamma} = \frac{C}{C + 1}, \quad (3)$$

where in the last equality we have made the connection to the cooperativity.

(Box 1). An obvious application of this regime is in exploiting the emitter’s saturable character to engineer non-classical states of light, such as individual photons. Unlike the spectral and dynamical features in photoluminescence, which also arise in entirely classical models, these states appear only in the truly quantum nonlinear regime. Two experimental signatures are non-classical intensity–intensity correlation measurements exhibiting  $g^{(2)}(0) \approx 0$ , the smoking gun of single-photon physics, and Hong–Ou–Mandel interferometry revealing photon indistinguishability, as shown with quantum dots<sup>91</sup> and defect centres<sup>53,92,93</sup>. Furthermore, using sequential driving, one can obtain multiphoton time-bin entangled states<sup>94</sup>, or, if memory levels are available, photon-cluster states<sup>95,96</sup>, which are a resource for measurement-based quantum computation<sup>9</sup>. Finally, this high-cooperativity regime is also the basis for implementing quantum phase switches as demonstrated for both trapped atoms<sup>97</sup> and solid-state emitters<sup>98</sup>, which can become a resource in photonics quantum technologies.

In the strong-coupling regime, when light–matter coupling overcomes losses ( $g > \kappa, \gamma$ ), the cavity modes strongly hybridize with the emitter to form a new quasiparticle, called a polariton, with a nonlinear energy-level structure. This can be seen explicitly by diagonalizing the Jaynes–Cummings Hamiltonian. Because the Hamiltonian conserves the total number of excitations  $n$ , its associated Hilbert space separates into one  $2 \times 2$  block for each value of  $n = 0, 1, 2, \dots$ . Each block results in two polaritonic branches with a Rabi splitting proportional

**Table 1 | Comparison of cavity modes**

Cavity (localized) modes	Type	$V/\lambda^3$	Q
 Defect cavity in 2D photonic crystals	Dielectric	1	$10^4$ – $10^6$
 Metallic bowtie nanoantenna	Metallic	$10^{-5}$ – $10^{-6}$	1–10
 Metal–dielectric cavity	Hybrid	$10^{-4}$ – $10^{-1}$	$10^2$ – $10^3$
 Subwavelength-variation refractive index	Dielectric	$10^{-3}$	$10^3$ – $10^5$

Illustrative values are given here, using estimated orders of magnitude. Specific values for different systems can be found in the primary literature.

to  $\sqrt{n}$ , which results in an anharmonic spectrum. These anticrossings are evident in photoluminescence spectra (or their complementary Rabi oscillations in the dynamics), as demonstrated in the first experiments using quantum dots in microcavities<sup>99–101</sup> or molecules in plasmonic nanoantennas<sup>71</sup> (Fig. 2c). One can also certify the strong-coupling regime with intensity correlation measurements<sup>63,102</sup>. These reveal a photon-blockade effect wherein light that is resonant with the first excited polariton mode is incapable of being absorbed (owing to the anharmonicity of the spectrum) and inducing transitions to further excited states, resulting in  $g^{(2)}(0) < 1$ . At the complementary regime, that is, when the laser is resonant with some of the multiphoton transitions, the system can filter the multiphoton component of the classical light pulses, as has been recently demonstrated in measuring the bunching of higher-order intensity correlations (Fig. 2d). Expected improvements in fabrication techniques and designs may result in an increase of cooperativities, enabling applications of the strong-coupling regime, such as the generation of multiphoton states of light<sup>103</sup> or the implementation of quantum non-demolition qubit readout and bosonic gates in the dispersive regime ( $g \ll |\omega_{eg} - \omega_a|$ ) (ref. 104).

The main figure of merit that characterizes the potential of both the weak- and strong-coupling regimes is the cooperativity  $C$ . Defect centres coupled to nanophotonic cavities<sup>53,105,106</sup> reach cooperativities within the  $C - O(10$ – $1000)$  range, expected to increase with fabrication improvements. Reaching such numbers with atomic systems is generally harder as it involves trapping them close to the surface. However, recent advances have shown that tweezers close to nanophotonic cavities and optical guiding techniques near whispering-gallery-mode resonators<sup>44</sup> may reach values of  $C \approx 70$  and  $C \approx 7$ , respectively.

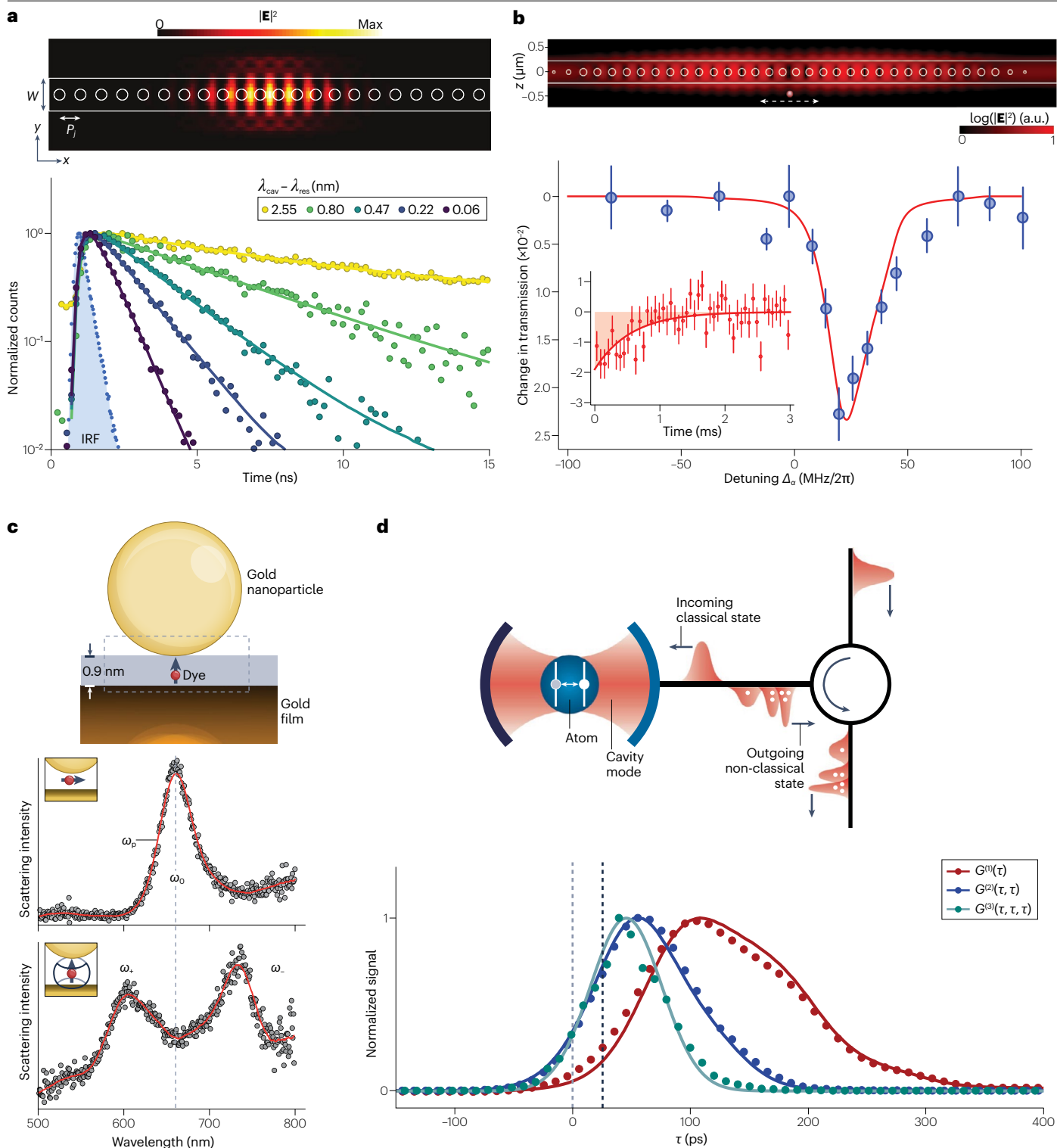
## Waveguide QED

Waveguide QED refers to a setup in which quantum emitters interact with a continuum of confined light modes propagating along one or two dimensions<sup>19</sup>. When the emitter's optical transition lies within the

band structure of the waveguide modes, the propagating nature of the modes leads to irreversible decay dynamics. Thus, the phenomenology, figures of merit and applications emergent in this configuration are very similar to those obtained in the weak-coupling regime of cavity QED. In the single-emitter regime, waveguides have a built-in channel to in/out-couple light, and the waveguide decay rate,  $\Gamma_{1D}$ , is enhanced not only by the subwavelength confinement of light but also through the reduction of the group velocity of light ( $v_g$ ) due to the refractive index of the material,  $\Gamma_{1D} \propto c/v_g$ , which can be reduced by periodically modulating the material. Furthermore, the propagation length of waveguide modes – how much they can travel before decaying into other modes – is also very long because of the reduced diffraction and, in the case of dielectrics, low absorption of the material. These conditions enable distant emitters to interact by exchanging photonic waveguide excitations.

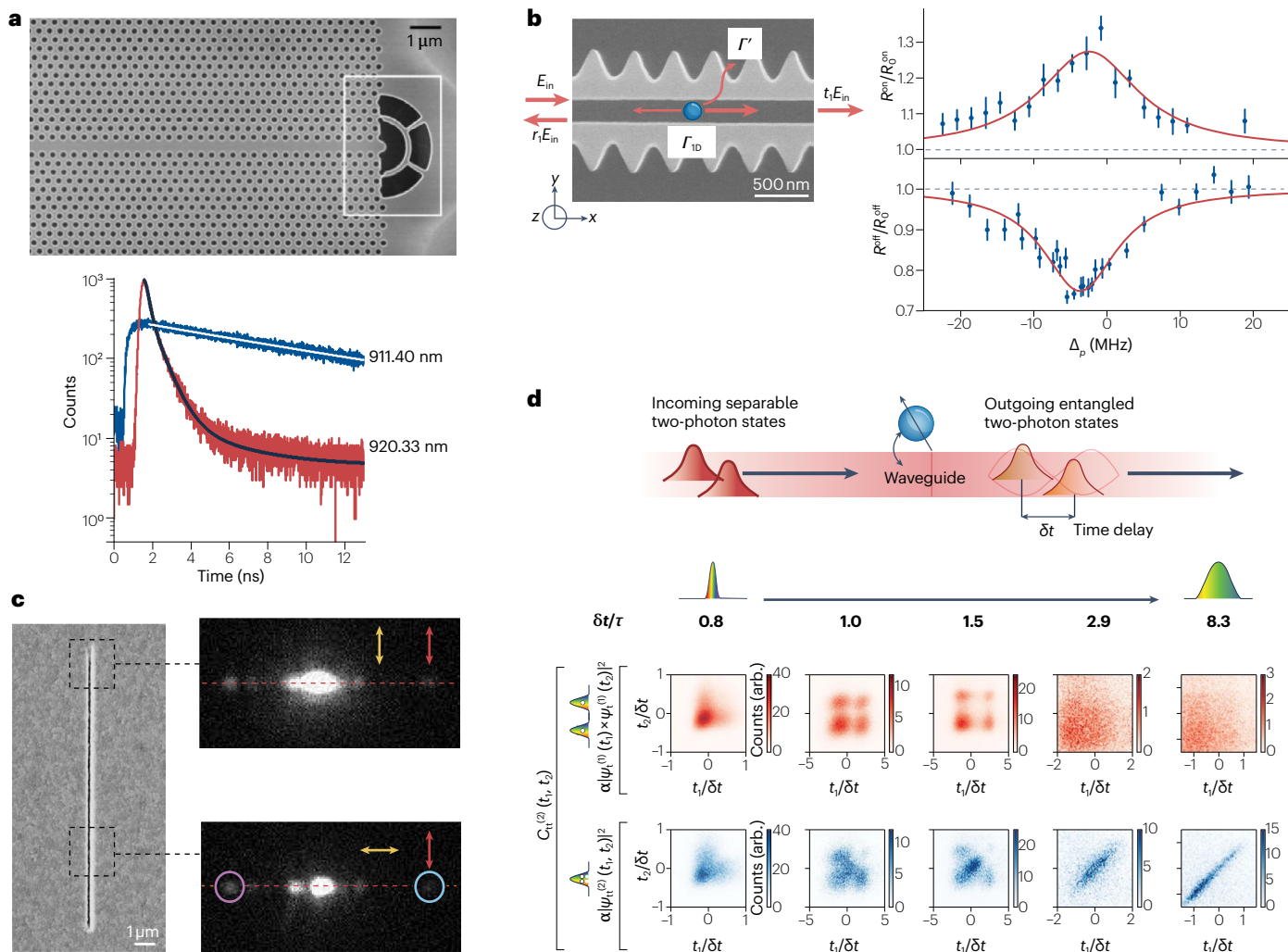
Figure 3 shows several waveguide QED realizations and the experimental signatures used to characterize them, such as emitter lifetime reduction (Fig. 3a), light sub-Poissonian statistics ( $g^{(2)}(0) < 1$ ) (Fig. 3b), real-space photoluminescence (Fig. 3c) or bunched multiphoton components ( $G^{(2)}(0) > G^{(2)}(t)$ ) (Fig. 3d). See also Table 2. Quantum dots<sup>64,107</sup> and defect centres<sup>25,108</sup> are the waveguide QED setups with the highest cooperativities. The combination of the slow-light enhancement in photonic-crystal waveguides and the emitter's integration in the material results in a cancellation of free-space emission, leading to  $C > 10$  for such setups. Pairing solid-state emitters with the strongly confined light from plasmonic waveguides also results in high cooperativities  $C \approx 5$ – $10$  (refs. 109,110). However, owing to the surface plasmons' short propagation length, it is challenging to connect multiple emitters together. Finally, trapped atoms near nanostructures show smaller cooperativities, with  $C \approx 0.05$ – $0.1$  for optical fibres<sup>31,35,37–40</sup> and  $C \approx 1$ – $2$  for photonic-crystal waveguides<sup>32</sup>, mainly owing to the difficulty of putting the atoms near the nanostructures. However, new waveguide and trapping designs show that prospects of reaching  $C - O(10)$  are realistic in the near term (see for example ref. 41). On the applications side, waveguide QED's main potential lies in generating non-classical states, such as single-photons<sup>111,112</sup> or more complex states of light exploiting multilevel structures<sup>113</sup>. Waveguide QED setups can also be used as quantum memories and as quantum links between quantum processors.

A relevant application of waveguide QED uses emitters to imprint phases and perform quantum operations on the propagating photons. This is best implemented in a chiral waveguide configuration<sup>15</sup>, where the emitters absorb and emit photons preferably along the same direction, affecting only their quantum state and not their direction of motion. Nanophotonics enables the design of a chiral waveguide QED regime in two complementary ways (Fig. 4). The first exploits the spin–orbit coupling of light<sup>114</sup> emerging from the polarization patterns of the subwavelength confined modes<sup>115–117</sup>, as demonstrated in photonic crystal waveguides<sup>117</sup> and optical fibres<sup>115,116</sup> (Fig. 4a,b). The second way requires engineering waveguide modes that propagate only along one direction, as is the case for edge modes in a topological photonic insulator<sup>118</sup> (Fig. 4c). Irrespective of the platform, the asymmetric emission into left- and right-moving modes opens a plethora of applications unavailable in standard waveguide QED setups, such as deterministic quantum state transfer with fully directional couplings<sup>119</sup>, or the passive quantum phase gates based on the scattering with emitters introduced above<sup>120</sup>. Besides, in systems with multiple topological edge states<sup>121–123</sup>, one can perform such operations within the topological protected channels.



**Fig. 2 | Nanophotonics cavity quantum electrodynamics (QED) realizations and experimental signatures. a**, Lifetime reduction of an emitter coupled to the cavity when changing their relative detuning in different colours. **b**, Cavity transmission line-broadening due to Purcell enhancement in the weak-coupling regime,  $\Delta$  being the cavity-emitter detuning. **c**, Spectrum for a molecular cavity QED setup in a weakly (strongly) coupled situation in the upper (lower) panel,

respectively. **d**, Photon-photon correlations  $G^{(1)}(\tau)$ ,  $G^{(2)}(\tau, \tau)$ ,  $G^{(2)}(\tau, \tau)$ ,  $G^{(3)}(\tau, \tau, \tau)$  show the separation of the multiphoton components (outgoing wavepacket) of a coherent pulse (incoming wavepacket) due to the interaction with a cavity QED system. Panel **a** adapted from ref. 105, CC BY 4.0. Panel **b** adapted with permission from ref. 33, AAAS. Panel **c** adapted from ref. 71, Springer Nature Limited. Panel **d** is adapted from ref. 182, CC BY 4.0.



**Fig. 3 | Nanophotonic waveguide QED realizations and experimental signatures.** **a**, A single quantum dot coupled to a dielectric photonic-crystal waveguide features lifetime reduction close to band edges (from blue to red). **b**, An alternative signature to demonstrate the coupling of an emitter (an atom, depicted in blue, that is trapped in the gap of a slow-light waveguide) is to measure the broadening of the linewidth in transmission ( $t$ ) or reflection ( $r$ ) as a function of the detuning  $\Delta_p$ . **c**, A single Nitrogen Vacancy centre coupled to a V-groove, metallic waveguide whose emission into the waveguide modes was evidenced by far-field imaging. Here, the yellow (red) arrow represents the excitation (collection) polarization. The circles indicate the ends of the waveguide.

**d**, Temporal correlations induced by photon–photon emitter-mediated interactions. The schematic picture depicts two incoming separable photonic wavepackets becoming entangled after their scattering with the emitter. The plots represent the measured time-resolved second-order correlation functions  $C_{tt}^{(2)}(t_1, t_2)$  for various pulse durations  $\delta t$  in the different columns relative to the QD lifetime and for two single photons from subsequently scattered pulses (upper row) and two photons contained in the same pulse (lower row). Panel **a** adapted with permission from ref. 107, APS. Panel **b** adapted from ref. 32, Springer Nature Limited. Panel **c** is adapted from ref. 110, CC BY 4.0. Panel **d** adapted from ref. 183, Springer Nature Limited.

Finally, let us mention another regime of photonic-crystal waveguides<sup>32,124</sup> that leads to qualitatively different phenomena. It consists of tuning the emitter’s optical transition in one of the photonic bandgaps of the waveguide modes. Since the late 1990s, it has been known that the presence of the band edges modifies spontaneous emission, leading to incomplete atomic relaxations<sup>125</sup> – termed fractional decay. Because the photons emitted in that scenario cannot propagate, they localize around the emitter, forming atom–photon bound states<sup>126–128</sup> that strongly renormalize the emitter’s frequency. Such renormalization, which was the experimental smoking gun



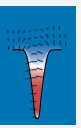
demonstrating the atom–photon bound-state regime<sup>124</sup>, can be further harnessed to engineer strong optical nonlinearities<sup>129</sup>.

## Collective effects

In the collective regime, many emitters are placed controllably near the photonic nanostructures, and the exchange of confined photons leads to long-range and versatile photon-mediated interactions between emitters. These interactions can be effectively controlled by engineering the nanostructures and tuning the coupling between the emitter and light. Irrespective of the localized or propagating nature of the



**Table 2 | Comparison of waveguide modes**

Waveguide (propagating) modes	Type	$L_{\text{prop}}/\lambda$
 Optical fibre	Dielectric	$10^3\text{--}10^4$
 Photonic-crystal waveguide	Dielectric	$10^3\text{--}10^4$
 V-groove plasmonic waveguide	Metallic	1–10

Illustrative values are given here, using estimated orders of magnitude. Specific values for different systems can be found in the primary literature.

photonic modes, the dynamics of the emitters separates into a coherent and a dissipative regime, depending on the relative detuning between the emitters' transition and the photonic modes (Box 2). Here, we use this division to discuss the emergent collective phenomena that can appear in these setups.

## Coherent regime

The coherent regime arises when the emitters' optical transitions are off-resonant with either the cavity or the waveguide modes, and the free-space decay does not dominate. In this situation, quantum emitters may interact by exchanging off-resonant or virtual photons. This process results in a perfectly coherent exchange of excitations between emitters at rate  $J_{i,j}$  described by the Hamiltonian in Box 2. Even if the cavity or waveguide exhibits photon loss, the photon-mediated interaction is mainly coherent, as the dissipative processes are strongly suppressed by the small photonic population during the exchange of virtual excitations.

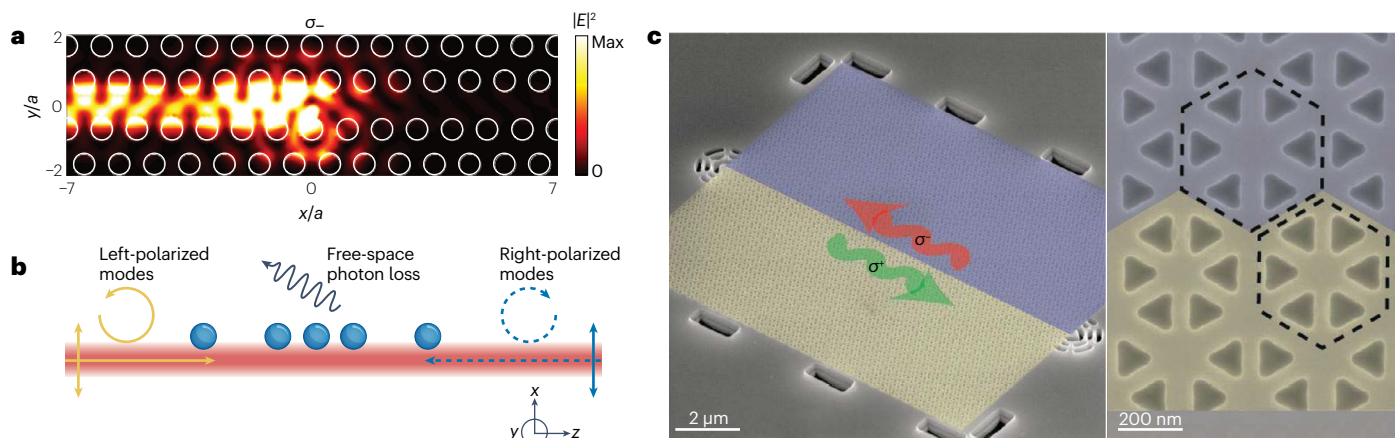
The shape of the coherent photon-mediated interactions  $J_{i,j}$  depends on the photonic mode and the light–matter coupling. For example, nanoscale single-mode cavities mediate naturally infinite-range

interactions<sup>5</sup>  $J_{i,j} \propto g(x_i)g(x_j)^*(\omega_0 - \omega_a)^{-1}$ , where the only spatial dependence comes from the individual coupling strength of each emitter. In photonic-crystal waveguides, the photon-mediated interactions acquire the shape of the atom–photon bound states forming in the individual emitter case<sup>126–128</sup>. Thus, for standard quadratic band-edge dispersions<sup>130,131</sup>, the photon-mediated interactions acquire an exponential shape,  $J_{i,j} \propto J e^{-|x_i - x_j|/L}$ , whose strength  $J$  and range ( $L$ ) depends on the distance between the optical transition and the band edge. In contrast, singular bandgaps lead to power-law decays  $J_{i,j} \propto 1/r^\alpha$  (refs. 132–134). Assuming access to additional emitter levels and laser-induced Raman-type transitions, one may not only change  $J$  and  $L$  dynamically<sup>130,131,135,136</sup>, but also transform the interaction from a spin-exchange to an Ising-type coupling, and thus engineer the couplings between qudits. Such interactions enable the design of quantum gates between emitters<sup>137</sup>, the simulation of frustrated spin Hamiltonians<sup>138</sup>, and more efficient variational quantum computing<sup>139</sup>, among other applications<sup>14</sup>. Although we only have indirect experimental evidence of the coherent regime in nanophotonics<sup>124</sup>, recent experiments in microwave photonic setups exemplify the potential of these ideas<sup>140,141</sup>.

Taking advantage of the fact that collective effects improve the effective coupling strength of an ensemble of quantum emitters  $N_e$  to a cavity mode by a factor  $\sqrt{N_e}$  (ref. 142), collective strong light–matter coupling has recently been used to manipulate matter excitations by vacuum fields<sup>143,144</sup>. Along this line, it has been demonstrated that charge<sup>145</sup> and energy transport<sup>146</sup> can be enhanced in organic materials, that site-selective chemical reactivity across a range of molecular systems can be tuned<sup>147</sup>, and that even collective phenomena emerging in macroscopic solid-state systems, such as superconductivity<sup>148</sup> and magnetic or electric order<sup>150</sup>, can be altered using cavity QED scenarios.

## Dissipative regime

In the complementary regime, that is, when the emitters' optical transitions are resonant either with the guided modes of the structure or with lossy single-mode cavities, the emitters also experience coherent photon exchanges between them at rates  $J_{i,j}$ . However, as these photons will eventually propagate away from the emitters, these coherent exchanges



**Fig. 4 | Chiral quantum optics in waveguide QED. a**, Spin–orbit coupling in photonic-crystal waveguides. A simulation of the electromagnetic field radiated by a quantum dot shows that a left-polarized dipole ( $\sigma_-$ ) emits only into the left-moving modes. **b**, Spin–orbit coupling in optical fibres. The left- (right-)polarized dipoles ( $\sigma_{-(+)}$ ) shown by yellow (blue) circular arrows are coupled to the right- (left-)moving

emission into the nanofibres. **c**, Engineering chiral propagating modes exploiting topological photonic structures. Here, the interface between the two photonic crystals supports helical edge states with opposite circular polarization. Panel **a** is reprinted from ref. 117, Springer Nature Limited. Panel **b** is reprinted from ref. 115, CC BY 4.0. Panel **c** is reprinted with permission from ref. 118, AAAS.

are unavoidably accompanied by collective dissipative terms  $\gamma_{ij}$ . Such dissipation results in the emitter's non-unitary evolution, a process that, in the regime with no retardation or memory effects of the bath, is captured by the Lindblad-type master equation in Box 2.

Again, the particular shape of the photon-mediated interactions, both  $J_{ij}$  and  $\gamma_{ij}$ , depends on the nature of the photonic mode and its coupling to the emitters. For example, if all emitters are coupled equally to the lossy cavity, then  $J_{ij} = 0$  and  $\gamma_{ij} = \Gamma_{\text{cav}}$ . The same can be obtained in waveguide QED setups if the emitters' position is commensurate with the wavelength of the photons mediating the interaction, since  $\gamma_{ij} + iJ_{ij}/2 = \Gamma_{\text{ID}} e^{ik_0|x_i - x_j|}$ . This situation in which all the emitters radiate in phase to the environment is known as the pure Dicke model<sup>151</sup>, which is the paradigm of collective dissipative effects. In this regime, the interference between the radiation of the different emitters causes certain states, dubbed sub(super)radiant states, to completely decouple (or decay with a collective factor) from (into) the cavity/waveguide modes. These states are interesting because, despite their non-unitary origin, they can still be harnessed for quantum technological applications such as the generation of qubit entanglement<sup>17,152,153</sup>, the design of quantum gates in decoherence-free subspaces<sup>154,155</sup>, and improving the figures of merit in the generation of states with large and fixed photon number<sup>156,157</sup>, among other applications. In fully asymmetric

chiral waveguides<sup>15,115-117</sup>, the photon-mediated interactions combine both a chiral coherent coupling  $J_{i,j} = i\Gamma_{\text{ID}}$  and the fully collective dissipative terms  $\gamma_{ij} = \Gamma_{\text{ID}}$ , which captures the non-reciprocity of the interactions<sup>158,159</sup>. Combining such collective decays with judicious driving schemes, one can obtain multipartite driven-dissipative entangled states<sup>153,160,161</sup> in the stationary state of the evolution.

Experimentally, several platforms can already produce the experimental signatures of this regime (Fig. 5). Such features can be the enhancement of the linewidth broadening for an increasing number of emitters due to the infinite-range collective dissipative couplings, or the equivalent in the time domain, that is, the acceleration of radiated power dynamics. Both features have been observed in atoms coupled to optical nanofibres, for example in ref. 31 (Fig. 5a) and ref. 162 (Fig. 5b), respectively. In the latter case, the acceleration has recently reached the truly many-body regime<sup>163</sup>, in which one observes the celebrated super-radiant bursts in the radiative power dynamics<sup>163</sup>. This is one of the first manifestations of many-body collective dissipative phenomena<sup>151</sup> beyond the linear regime. Apart from superradiant effects, an equally important collective phenomenon is subradiance which manifests as a linewidth narrowing of certain entangled emitter states, as observed in a cavity QED setup with two Silicon Vacancy centres<sup>164</sup> (Fig. 5c). Another complementary manifestation of such subradiant states is the lifetime

## Box 2

### Coherent versus dissipative interactions

The coupling of quantum emitters to a common localized or propagating photonic mode induces effective photon-mediated interactions between them. The nature and shape of these interactions depend strongly on the relative detuning between the optical transition of the emitters and the energy of the photonic modes mediating the interactions: off-resonant photons (in blue) lead to coherent interactions between the emitters, whereas resonant ones (in red) lead also to individual and collective decays (see parts **a** and **b** of the figure). In free space, both of these appear simultaneously and cannot be engineered. However, when the atoms are placed near nanophotonic cavities or waveguides, such free-space interactions can be further modified (and even neglect this channel if cooperativities are large enough). In the coherent or dispersive regime (see part **b** of the figure), that is, when the optical transition is very far from any resonant photonic mode ( $|\omega_{\text{eg}} - \omega_{\text{a}}| \gg g$  in cavity QED or  $|\omega_{\text{eg}} - \omega_{\text{edge}}| \gg g$  in waveguide QED setups, where  $g$  is the coupling strength), the dynamics mediated by the off-resonant photons is purely coherent and governed by a Hamiltonian:

$$H_{\text{eff}} = \sum_{i,j} J_{i,j} \sigma_i^{\dagger} \sigma_j \quad (4)$$

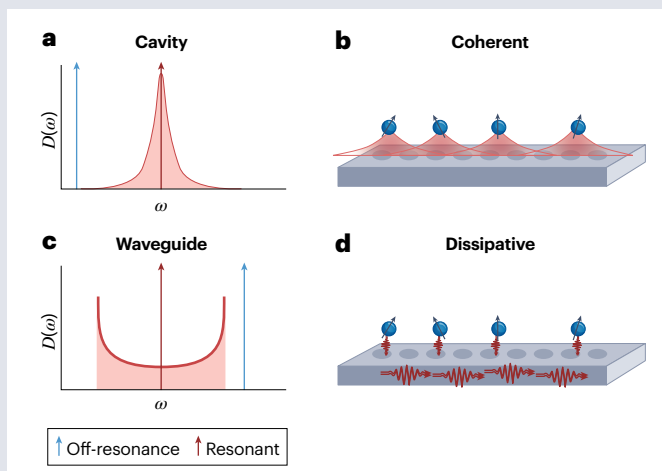
where  $J_{ij}$  depends on the atomic position in cavity QED and on the underlying photonic structure in waveguide QED. This coherent regime is interesting because the couplings  $J_{ij}$  can give rise to strong optical nonlinearities, or induce multiqubit entangling gates that can be harnessed for quantum simulation or variational quantum algorithms.

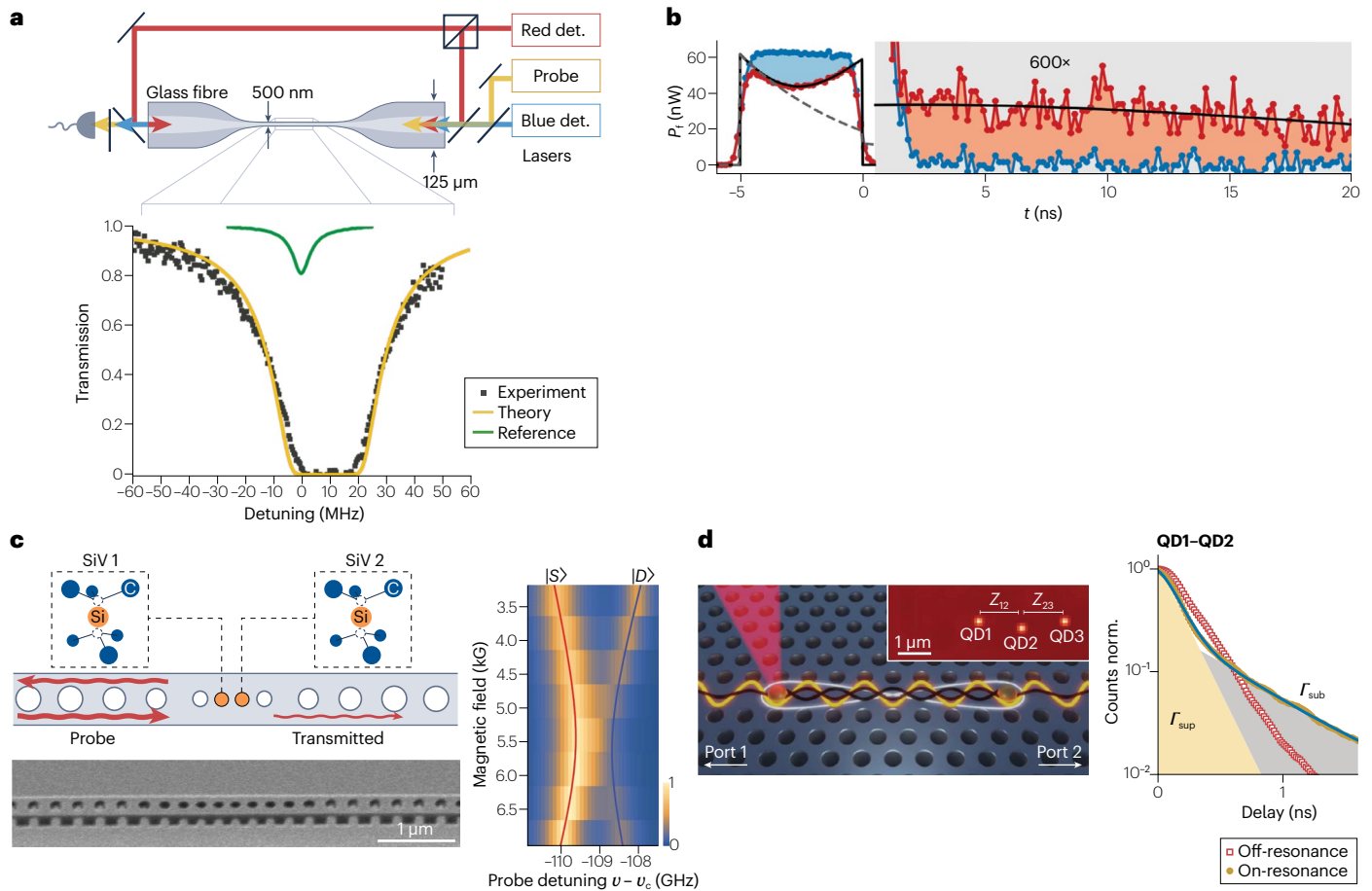
In the dissipative regime (see part **d** of the figure), which occurs when the energy of the emitters lies close to the band or cavity

modes, the dynamics induced is non-unitary and can be described by an effective master equation:

$$\frac{d\rho}{dt} = i \left[ \rho, \sum_{i,j} J_{i,j} \sigma_i^{\dagger} \sigma_j \right] + \sum_{i,j} \frac{\gamma_{i,j}}{2} (2\sigma_i \rho \sigma_j^{\dagger} - \sigma_i^{\dagger} \sigma_i \rho - \rho \sigma_j^{\dagger} \sigma_j), \quad (5)$$

Despite their dissipative nature, these collective decays  $\gamma_{ij}$  are also the source of interesting phenomena such as the renormalization of the lifetime of certain collective atomic states, the 'super/subradiant' states. Counterintuitively, these states can be used to protect quantum information in decoherence-free subspaces or enhance the emission into certain channels.





**Fig. 5 | Collective effects in the dissipative regime.** **a**, Attenuation of the transmission due to collective effects with atoms trapped with red and blue detuned (det) lasers near an optical nanofibre. Black dots correspond to the measurement data, red line to a theoretical fit, and the green line is the measurement of the atomic ensemble not coupled to the waveguide. **b**, Dynamics of the power of a fibre-guided, resonant probe pulse transmitted through about 300 atoms. Red dots indicate the measured data when atoms are coupled to the waveguide, whereas the blue line is the reference measurement without atoms. The upper panel is a schematic figure on the propagation of the light as it interacts with each atom until arriving to the

photo-detector. **c**, Observation of photon-mediated interactions through the anticrossing and linewidth changes of the symmetric,  $|S\rangle$ , and antisymmetric,  $|D\rangle$ , states in the spectrum of two defect centres in a nanophotonic cavity as a function of the probe detuning ( $\nu - \nu_c$ ). **d**, Lifetime modification due to the long-range dissipative interactions measured with quantum dot (QD) emitters coupled to photonic-crystal waveguides.  $\Gamma_{\text{sup(sub)}}$  corresponds to the lifetime of the super (sub) radiant states. Panel **a** adapted with permission from ref. 31, APS. Panel **b** adapted with permission from ref. 162, APS. Panel **c** adapted with permission from ref. 164, AAAS. Panel **d** adapted with permission from ref. 165, AAAS.

enhancement, as recently observed for pairs of quantum dots coupled to photonic-crystal waveguides<sup>165</sup> (Fig. 5d).

## Outlook

The past decade has witnessed tremendous progress in the development of quantum nanophotonic interfaces, motivated by outstanding opportunities for quantum technological applications. This rapid progress has enabled the field to demonstrate proof-of-principle quantum cooperative phenomena in very different platforms<sup>45,162–165</sup>. Based on upcoming improvements in nanofabrication, design<sup>41,42</sup> and trapping techniques<sup>46,50,51</sup>, we expect that the next decade will be the one in which quantum nanophotonics will make breakthroughs in specific quantum technological applications. At the forefront, rapidly improving cooperativities shall enable the design of fast, deterministic or probabilistic quantum gates in nanophotonic devices, enabling the processing of quantum information. Combining these quantum

operations with the possibility of out-coupling propagating photonic modes makes quantum nanophotonic devices a relevant candidate for implementing nodes in quantum networks<sup>36</sup> or establishing quantum links between quantum processors. Other exciting directions to explore in the following years involve designing nanophotonic devices that simultaneously exploit superradiance and free-space subradiance. This combination, termed ‘selective radiance’, will improve the figures of merit of single-photon emission and absorption<sup>166</sup>, aiding the implementation of quantum memories and the generation of complex states of light and matter for quantum metrological applications<sup>156,157,167</sup>. Furthermore, the shortening of timescales due to superradiance will severely challenge the quantum optics Born–Markov approximation. This regime may result in opportunities to obtain driven-dissipative phases or transient evolutions impossible to obtain in non-retarded situations<sup>168</sup>. The ultrastrong coupling regime<sup>169,170</sup> is a different way to challenge the existing approximations, pushing light–matter

interaction to values at which the emitter and photonic degrees of freedom hybridize. These situations enable new nonlinear phenomena at the single-photon level<sup>171</sup>, or even new effective regimes of interaction between emitters<sup>172–174</sup>. An alternative route for challenging the standard approximations consists in coupling the nanophotonic structures to new matter and photonic quasiparticles, such as excitons or phonons<sup>175–177</sup>. Another intriguing question is to explore whether one can exploit topological photonic systems to preserve the entanglement generation in such circuits<sup>123,178–180</sup>. Finally, the improvements in the confinement of light might make single-photon interactions using bulk nonlinearities sizeable, avoiding the need for integrating emitters to obtain quantum phenomena, and thus opening completely new operating regimes<sup>181</sup>.

Published online: 25 January 2024

## References

- Kimble, H. J. The quantum internet. *Nature* **453**, 1023–1030 (2008).
- Ekert, A. K. Quantum cryptography based on Bell's theorem. *Phys. Rev. Lett.* **67**, 661–663 (1991).
- Reiserer, A. Colloquium: Cavity-enhanced quantum network nodes. *Rev. Mod. Phys.* **94**, 041003 (2022).
- Bloch, I., Dalibard, J. & Zwinger, W. Many-body physics with ultracold gases. *Rev. Mod. Phys.* **80**, 885–964 (2008).
- Ritsch, H., Domokos, P., Brennecke, F. & Esslinger, T. Cold atoms in cavity-generated dynamical optical potentials. *Rev. Mod. Phys.* **85**, 553–601 (2013).
- Giovannetti, V., Lloyd, S. & Maccone, L. Advances in quantum metrology. *Nat. Photon.* **5**, 222 (2011).
- Gottesman, D., Kitaev, A. & Preskill, J. Encoding a qubit in an oscillator. *Phys. Rev. A* **64**, 012310 (2001).
- Grimsmo, A. L. & Puri, S. Quantum error correction with the Gottesman–Kitaev–Preskill code. *PRX Quantum* **2**, 020101 (2021).
- Briegel, H. J., Browne, D. E., Dür, W., Raussendorf, R. & den Nest, M. Measurement-based quantum computation. *Nat. Phys.* **5**, 19 (2009).
- Haroche, S. Nobel lecture: Controlling photons in a box and exploring the quantum to classical boundary. *Rev. Mod. Phys.* **85**, 1083–1102 (2013).
- Hammerer, K., Sørensen, A. S. & Polzik, E. S. Quantum interface between light and atomic ensembles. *Rev. Mod. Phys.* **82**, 1041–1093 (2010).
- Saffman, M., Walker, T. G. & Mølmer, K. Quantum information with Rydberg atoms. *Rev. Mod. Phys.* **82**, 2313–2363 (2010).
- Lodahl, P., Mahmoodian, S. & Stobbe, S. Interfacing single photons and single quantum dots with photonic nanostructures. *Rev. Mod. Phys.* **87**, 347–400 (2015).
- Chang, D. E., Douglas, J. S., González-Tudela, A., Hung, C.-L. & Kimble, H. J. Colloquium: Quantum matter built from nanoscopic lattices of atoms and photons. *Rev. Mod. Phys.* **90**, 031002 (2018).
- Lodahl, P. et al. Chiral quantum optics. *Nature* **541**, 473 (2017).
- Dzsojjan, D., Sørensen, A. S. & Fleischhauer, M. Quantum emitters coupled to surface plasmons of a nanowire: a Green's function approach. *Phys. Rev. B* **82**, 75427 (2010).
- Gonzalez-Tudela, A. et al. Entanglement of two qubits mediated by one-dimensional plasmonic waveguides. *Phys. Rev. Lett.* **106**, 020501 (2011).
- Ozawa, T. et al. Topological photonics. *Rev. Mod. Phys.* **91**, 15006 (2019).
- Sheremet, A. S., Petrov, M. I., Iorsh, I. V., Poshakinskiy, A. V. & Poddubny, A. N. Waveguide quantum electrodynamics: collective radiance and photon–photon correlations. *Rev. Mod. Phys.* **95**, 015002 (2023).
- Tame, M. S. et al. Quantum plasmonics. *Nat. Phys.* **9**, 329–340 (2013).
- Pelton, M. Modified spontaneous emission in nanophotonic structures. *Nat. Photon.* **9**, 427–435 (2015).
- Doherty, M. W. et al. The nitrogen-vacancy colour centre in diamond. *Phys. Rep.* **528**, 1–45 (2013).
- Bradac, C., Gao, W., Forneris, J., Trusheim, M. E. & Aharonovich, I. Quantum nanophotonics with group IV defects in diamond. *Nat. Commun.* **10**, 5625 (2019).
- Castelletto, S. & Boretti, A. Silicon carbide color centers for quantum applications. *J. Phys. Photonics* **2**, 022001 (2020).
- Gritsch, A., Weiss, L., Früh, J., Rinner, S. & Reiserer, A. Narrow optical transitions in erbium-implanted silicon waveguides. *Phys. Rev. X* **12**, 041009 (2022).
- Durand, A. et al. Broad diversity of near-infrared single-photon emitters in silicon. *Phys. Rev. Lett.* **126**, 083602 (2021).
- Zhong, T. & Goldner, P. Emerging rare-earth doped material platforms for quantum nanophotonics. *Nanophotonics* **8**, 2003–2015 (2019).
- Xia, F., Wang, H., Xiao, D., Dubey, M. & Ramasubramanian, A. Two-dimensional material nanophotonics. *Nat. Photon.* **8**, 899–907 (2014).
- Reserbat-Plantey, A. et al. Quantum nanophotonics in two-dimensional materials. *ACS Photonics* **8**, 85–101 (2021).
- Toninelli, C. et al. Single organic molecules for photonic quantum technologies. *Nat. Mater.* **20**, 1615–1628 (2021).
- Vetsch, E. et al. Optical interface created by laser-cooled atoms trapped in the evanescent field surrounding an optical nanofiber. *Phys. Rev. Lett.* **104**, 203603 (2010).
- Goban, A. et al. Atom–light interactions in photonic crystals. *Nat. Commun.* **5**, 3808 (2014).
- Thompson, J. D. et al. Coupling a single trapped atom to a nanoscale optical cavity. *Science* **340**, 1202–1205 (2013).
- Béguin, J.-B. et al. Generation and detection of a sub-Poissonian atom number distribution in a one-dimensional optical lattice. *Phys. Rev. Lett.* **113**, 263603 (2014).
- Solano, P., Barberis-Blostein, P., Fatemi, F. K., Orozco, L. A. & Rolston, S. L. Super-radiance reveals infinite-range dipole interactions through a nanofiber. *Nat. Commun.* **8**, 1857 (2017).
- Reiserer, A. & Rempe, G. Cavity-based quantum networks with single atoms and optical photons. *Rev. Mod. Phys.* **87**, 1379–1418 (2015).
- Goban, A. et al. Demonstration of a state-insensitive, compensated nanofiber trap. *Phys. Rev. Lett.* **109**, 33603 (2012).
- Corzo, N. V. et al. Large Bragg reflection from one-dimensional chains of trapped atoms near a nanoscale waveguide. *Phys. Rev. Lett.* **117**, 133603 (2016).
- Sørensen, H. L. et al. Coherent backscattering of light off one-dimensional atomic strings. *Phys. Rev. Lett.* **117**, 133604 (2016).
- Corzo, N. V. et al. Waveguide-coupled single collective excitation of atomic arrays. *Nature* **566**, 359–362 (2019).
- Bouscal, A. et al. Systematic design of a robust half-W1 photonic crystal waveguide for interfacing slow light and trapped cold atoms. Preprint at <https://arxiv.org/abs/2301.04675v1> (2023).
- Fayard, N. et al. Asymmetric comb waveguide for strong interactions between atoms and light. Preprint at <https://arxiv.org/abs/2201.02507v1> (2022).
- Béguin, J. B. et al. Reduced volume and reflection for bright optical tweezers with radial Laguerre–Gauss beams. *Proc. Natl. Acad. Sci. USA* **117**, 26109–26117 (2020).
- Zhou, X., Tamura, H., Chang, T.-H. & Hung, C.-L. Coupling single atoms to a nanophotonic whispering-gallery-mode resonator via optical guiding. *Phys. Rev. Lett.* **130**, 103601 (2023).
- Samutpraphoot, P. et al. Strong coupling of two individually controlled atoms via a nanophotonic cavity. *Phys. Rev. Lett.* **124**, 063602 (2020).
- Dordevic, T. et al. Entanglement transport and a nanophotonic interface for atoms in optical tweezers. *Science* **373**, 1511–1514 (2021).
- Endres, M. et al. Atom-by-atom assembly of defect-free one-dimensional cold atom arrays. *Science* **354**, 1024–1027 (2016).
- Barredo, D. et al. Coherent excitation transfer in a spin chain of three Rydberg atoms. *Phys. Rev. Lett.* **114**, 113002 (2015).
- Barredo, D., De Léséleuc, S., Lienhard, V., Lahaye, T. & Browaeys, A. An atom-by-atom assembler of defect-free arbitrary two-dimensional atomic arrays. *Science* **354**, 1021–1023 (2016).
- Menon, S. G., Glachman, N., Pompili, M., Dibos, A. & Bernien, H. An integrated atom array–nanophotonic chip platform with background-free imaging. Preprint at <https://arxiv.org/abs/2311.02153> (2023).
- Zhou, X., Tamura, H., Chang, T.-H. & Hung, C.-L. Trapped atoms and superradiance on an integrated nanophotonic microring circuit. Preprint at <https://arxiv.org/abs/2312.14318> (2023).
- Sipahigil, A. et al. An integrated diamond nanophotonics platform for quantum-optical networks. *Science* **354**, 847–850 (2016).
- Qurari, S. et al. Indistinguishable telecom band photons from a single erbium ion in the solid state. *Nature* **620**, 977–981 (2023).
- Wolfowicz, G. et al. Quantum guidelines for solid-state spin defects. *Nat. Rev. Mater.* **6**, 906–925 (2021).
- Santori, C., Fattal, D., Vukovick, J., Solomon, G. S. & Yamamoto, Y. Indistinguishable photons from a single-photon device. *Nature* **419**, 594–597 (2002).
- Zaporski, L. et al. Ideal refocusing of an optically active spin qubit under strong hyperfine interactions. *Nat. Nanotechnol.* **18**, 257–263 (2023).
- Faez, S., Türschmann, P., Haakh, H. R., Göttinger, S. & Sandoghdar, V. Coherent interaction of light and single molecules in a dielectric nanoguide. *Phys. Rev. Lett.* **113**, 213601 (2014).
- Wang, D. et al. Turning a molecule into a coherent two-level quantum system. *Nat. Phys.* **15**, 483–489 (2019).
- Bhaskar, M. K. et al. Experimental demonstration of memory-enhanced quantum communication. *Nature* **580**, 60–64 (2020).
- Ruf, M., Wan, N. H., Choi, H., Englund, D. & Hanson, R. Quantum networks based on color centers in diamond. *J. Appl. Phys.* **130**, 070901 (2021).
- Fermi, E. Quantum theory of radiation. *Rev. Mod. Phys.* **4**, 87 (1932).
- Cohen-Tannoudji, C., Dupont-Roc, J. & Grynberg, G. *Atom–Photon Interactions* (Wiley, 1998).
- Hennessy, K. et al. Quantum nature of a strongly coupled single quantum dot–cavity system. *Nature* **445**, 896–899 (2007).
- Laucht, A. et al. A waveguide-coupled on-chip single-photon source. *Phys. Rev. X* **2**, 11014 (2012).
- Weiss, L., Gritsch, A., Merkel, B. & Reiserer, A. Erbium dopants in nanophotonic silicon waveguides. *Optica* **8**, 40–41 (2021).
- Robinson, J. T., Manolatu, C., Chen, L. & Lipson, M. Ultrasmall mode volumes in dielectric optical microcavities. *Phys. Rev. Lett.* **95**, 143901 (2005).

67. Hu, S. et al. Experimental realization of deep-subwavelength confinement in dielectric optical resonators. *Sci. Adv.* **4**, eaat2355 (2018).
68. Albrechtsen, M. et al. Nanometer-scale photon confinement in topology-optimized dielectric cavities. *Nat. Commun.* **13**, 6281 (2022).
69. Chang, W.-H. et al. Efficient single-photon sources based on low-density quantum dots in photonic-crystal nanocavities. *Phys. Rev. Lett.* **96**, 117401 (2006).
70. Chang, D. E., Sørensen, A. S., Demler, E. A. & Lukin, M. D. A single-photon transistor using nanoscale surface plasmons. *Nature* **3**, 807–812 (2007).
71. Chikkaraddy, R. et al. Single-molecule strong coupling at room temperature in plasmonic nanocavities. *Nature* **535**, 127 (2016).
72. Benz, F. et al. Single-molecule optomechanics in ‘picocavities’. *Science* **354**, 726–729 (2016).
73. Kelkar, H. et al. Sensing nanoparticles with a cantilever-based scannable optical cavity of low finesse and sub- $\lambda^3$  volume. *Phys. Rev. Appl.* **4**, 054010 (2015).
74. Wang, D. et al. Coherent coupling of a single molecule to a scanning Fabry–Perot microcavity. *Phys. Rev. X* **7**, 021014 (2017).
75. Shlesinger, I., Vandersmissen, J., Oksenberg, E., Verhagen, E. & Koenderink, A. F. Hybrid cavity-antenna architecture for strong and tunable sideband-selective molecular Raman scattering enhancement. Preprint at <https://arxiv.org/abs/2306.17286v1> (2023).
76. Smith, D. R., Pendry, J. B. & Wiltshire, M. C. Metamaterials and negative refractive index. *Science* **305**, 788–792 (2004).
77. Veselago, V. G. The electrodynamics of substances with simultaneously negative values of  $\epsilon$  and  $\mu$ . *Sov. Phys. Usp.* **10**, 509 (1968).
78. Pendry, J. B., Holden, A. J., Robbins, D. J. & Stewart, W. J. Magnetism from conductors and enhanced nonlinear phenomena. *IEEE Trans. Microw. Theory Tech.* **47**, 2075–2084 (1999).
79. Bekenstein, R. et al. Quantum metasurfaces with atom arrays. *Nat. Phys.* **16**, 676–681 (2020).
80. Patti, T. L., Wild, D. S., Shahmoon, E., Lukin, M. D. & Yelin, S. F. Controlling interactions between quantum emitters using atom arrays. *Phys. Rev. Lett.* **126**, 223602 (2021).
81. Fernández-Fernández, D. & González-Tudela, A. Tunable directional emission and collective dissipation with quantum metasurfaces. *Phys. Rev. Lett.* **128**, 113601 (2022).
82. Ozawa, T. et al. Topological photonics. *Rev. Mod. Phys.* **91**, 015006 (2019).
83. Haldane, F. D. M. & Raghu, S. Possible realization of directional optical waveguides in photonic crystals with broken time-reversal symmetry. *Phys. Rev. Lett.* **100**, 13904 (2008).
84. Wang, Z., Chong, Y., Joannopoulos, J. D. & Soljačić, M. Observation of unidirectional backscattering-immune topological electromagnetic states. *Nature* **461**, 772 (2009).
85. Rostawska, A. et al. Mapping Lamb, Stark, and Purcell effects at a chromophore–picocavity junction with hyper-resolved fluorescence microscopy. *Phys. Rev. X* **12**, 011012 (2022).
86. Andersen, M. L., Stobbe, S., Sørensen, A. S. & Lodahl, P. Strongly modified plasmon–matter interaction with mesoscopic quantum emitters. *Nat. Phys.* **7**, 215–218 (2011).
87. Pscherer, A. et al. Single-molecule vacuum Rabi splitting: four-wave mixing and optical switching at the single-photon level. *Phys. Rev. Lett.* **127**, 133603 (2021).
88. Jaynes, E. & Cummings, F. W. Comparison of quantum and semiclassical radiation theories with application to the beam maser. *Proc. IEEE* **51**, 89–109 (1963).
89. Gérard, J.-M. et al. Enhanced spontaneous emission by quantum boxes in a monolithic optical microcavity. *Phys. Rev. Lett.* **81**, 1110 (1998).
90. Bayer, M. et al. Inhibition and enhancement of the spontaneous emission of quantum dots in structured microresonators. *Phys. Rev. Lett.* **86**, 3168 (2001).
91. Somaschi, N. et al. Near-optimal single-photon sources in the solid state. *Nat. Photon.* **10**, 340–345 (2016).
92. Siphahigil, A. et al. Indistinguishable photons from separated silicon-vacancy centers in diamond. *Phys. Rev. Lett.* **113**, 113602 (2014).
93. Knall, E. N. et al. Efficient source of shaped single photons based on an integrated diamond nanophotonic system. *Phys. Rev. Lett.* **129**, 053603 (2022).
94. Wein, S. C. et al. Photon-number entanglement generated by sequential excitation of a two-level atom. *Nat. Photon.* **16**, 374–379 (2022).
95. Schwartz, I. et al. Deterministic generation of a cluster state of entangled photons. *Science* **354**, 434–437 (2016).
96. Istrati, D. et al. Sequential generation of linear cluster states from a single photon emitter. *Nat. Commun.* **11**, 5501 (2020).
97. Tiecke, T. G. et al. Nanophotonic quantum phase switch with a single atom. *Nature* **508**, 241–244 (2014).
98. Sun, S., Kim, H., Solomon, G. S. & Waks, E. A quantum phase switch between a single solid-state spin and a photon. *Nat. Nanotechnol.* **11**, 539–544 (2016).
99. Reithmaier, J. P. et al. Strong coupling in a single quantum dot–semiconductor microcavity system. *Nature* **432**, 197 (2004).
100. Yoshie, T. et al. Vacuum Rabi splitting with a single quantum dot in a photonic crystal nanocavity. *Nature* **432**, 200–203 (2004).
101. Peter, E. et al. Exciton-photon strong-coupling regime for a single quantum dot embedded in a microcavity. *Phys. Rev. Lett.* **95**, 67401 (2005).
102. Reinhard, A. et al. Strongly correlated photons on a chip. *Nat. Photon.* **6**, 93–96 (2012).
103. Muñoz, C. S. et al. Emitters of  $N$ -photon bundles. *Nat. Photon.* **8**, 550–555 (2014).
104. Blais, A., Grimsmo, A. L., Girvin, S. M. & Wallraff, A. Circuit quantum electrodynamics. *Rev. Mod. Phys.* **93**, 025005 (2021).
105. Rugar, A. E. et al. Quantum photonic interface for tin-vacancy centers in diamond. *Phys. Rev. X* **11**, 031021 (2021).
106. Kuruma, K. et al. Coupling of a single tin-vacancy center to a photonic crystal cavity in diamond. *Appl. Phys. Lett.* **118**, 230601 (2021).
107. Arcari, M. et al. Near-unity coupling efficiency of a quantum emitter to a photonic crystal waveguide. *Phys. Rev. Lett.* **113**, 093603 (2014).
108. Bhaskar, M. K. et al. Quantum nonlinear optics with a germanium-vacancy color center in a nanoscale diamond waveguide. *Phys. Rev. Lett.* **118**, 223603 (2017).
109. Akimov, I. A., Andrews, J. T. & Henneberger, F. Stimulated emission from the biexciton in a single self-assembled [III-V] quantum dot. *Phys. Rev. Lett.* **96**, 67401 (2006).
110. Bermúdez-Ureña, E. et al. Coupling of individual quantum emitters to channel plasmons. *Nat. Commun.* **6**, 7883 (2015).
111. Uppu, R. et al. Scalable integrated single-photon source. *Sci. Adv.* **6**, eabc8268 (2020).
112. Uppu, R., Midolo, L., Zhou, X., Carolan, J. & Lodahl, P. Quantum-dot-based deterministic photon–emitter interfaces for scalable photonic quantum technology. *Nat. Nanotechnol.* **16**, 1308–1317 (2021).
113. Østfeldt, F. T. et al. On-demand source of dual-rail photon pairs based on chiral interaction in a nanophotonic waveguide. *PRX Quantum* **3**, 020363 (2022).
114. Bliokh, K. Y., Rodríguez-Fortuño, F. J., Nori, F. & Zayats, A. V. Spin–orbit interactions of light. *Nat. Photon.* **9**, 796–808 (2015).
115. Mitsch, R., Sayrin, C., Albrecht, B., Schneeweiss, P. & Rauschenbeutel, A. Quantum state-controlled directional spontaneous emission of photons into a nanophotonic waveguide. *Nat. Commun.* **5**, 5713 (2014).
116. Sayrin, C. et al. Nanophotonic optical isolator controlled by the internal state of cold atoms. *Phys. Rev. X* **5**, 41036 (2015).
117. Söllner, I. et al. Deterministic photon–emitter coupling in chiral photonic circuits. *Nat. Nanotechnol.* **10**, 775–778 (2015).
118. Barik, S. et al. A topological quantum optics interface. *Science* **359**, 666–668 (2018).
119. Cirac, J. I., Zoller, P., Kimble, H. J. & Mabuchi, H. Quantum state transfer and entanglement distribution among distant nodes in a quantum network. *Phys. Rev. Lett.* **78**, 3221 (1997).
120. Schirinski, B., Lamaison, M. & Sørensen, A. S. Passive quantum phase gate for photons based on three level emitters. *Phys. Rev. Lett.* **129**, 130502 (2022).
121. Skirlo, S. A., Lu, L. & Soljačić, M. Multimode one-way waveguides of large Chern numbers. *Phys. Rev. Lett.* **113**, 113904 (2014).
122. Skirlo, S. A. et al. Experimental observation of large Chern numbers in photonic crystals. *Phys. Rev. Lett.* **115**, 253901 (2015).
123. Vega, C., Porras, D. & González-Tudela, A. Topological multimode waveguide QED. *Phys. Rev. Res.* **5**, 023031 (2023).
124. Hood, J. D. et al. Atom–atom interactions around the band edge of a photonic crystal waveguide. *Proc. Natl Acad. Sci. USA* **113**, 10507–10512 (2016).
125. John, S. & Quang, T. Spontaneous emission near the edge of a photonic band gap. *Phys. Rev. A* **50**, 1764–1769 (1994).
126. Bykov, V. P. Spontaneous emission from a medium with a band spectrum. *Sov. J. Quantum Electron.* **4**, 861 (1975).
127. Kurizki, G. Two-atom resonant radiative coupling in photonic band structures. *Phys. Rev. A* **42**, 2915–2924 (1990).
128. John, S. & Wang, J. Quantum optics of localized light in a photonic band gap. *Phys. Rev. B* **43**, 12772–12789 (1991).
129. Shahmoon, E., Grišins, P., Stimming, H. P., Mazets, I. & Kurizki, G. Highly nonlocal optical nonlinearities in atoms trapped near a waveguide. *Optica* **3**, 725–733 (2016).
130. Douglas, J. S. et al. Quantum many-body models with cold atoms coupled to photonic crystals. *Nat. Photon.* **9**, 326–331 (2015).
131. González-Tudela, A., Hung, C.-L., Chang, D. E., Cirac, J. I. & Kimble, H. J. Subwavelength vacuum lattices and atom–atom interactions in two-dimensional photonic crystals. *Nat. Photon.* **9**, 320–325 (2015).
132. González-Tudela, A. & Cirac, J. Exotic quantum dynamics and purely long-range coherent interactions in Dirac conelike baths. *Phys. Rev. A* **97**, 043831 (2018).
133. Perczel, J. & Lukin, M. D. Theory of dipole radiation near a Dirac photonic crystal. *Phys. Rev. A* **101**, 033822 (2020).
134. Navarro-Barón, E. P., Vinck-Posada, H. & González-Tudela, A. Photon-mediated interactions near a Dirac photonic crystal slab. *ACS Photonics* **8**, 3209–3217 (2021).
135. Hung, C.-L., González-Tudela, A., Cirac, J. I. & Kimble, H. J. Quantum spin dynamics with pairwise-tunable, long-range interactions. *Proc. Natl Acad. Sci. USA* **113**, E4946–E4955 (2016).
136. Tabares, C., Zohar, E. & González-Tudela, A. Tunable photon-mediated interactions between spin-1 systems. *Phys. Rev. A* <https://doi.org/10.1103/PhysRevA.106.033705> (2022).
137. Kim, J., Yu, S. & Park, N. Universal design platform for an extended class of photonic Dirac cones. *Phys. Rev. Appl.* **13**, 044015 (2020).
138. Bello, M., Platero, G. & González-Tudela, A. Spin many-body phases in standard- and topological-waveguide QED simulators. *PRX Quantum* **3**, 010336 (2022).
139. Tabares, C., Heras, A. Mdl, Tagliacozzo, L., Porras, D. & González-Tudela, A. Variational quantum simulators based on waveguide QED. *Phys. Rev. Lett.* **131**, 073602 (2023).
140. Scigliuzzo, M. et al. Controlling atom–photon bound states in an array of Josephson-junction resonators. *Phys. Rev. X* **12**, 031036 (2022).
141. Zhang, X., Kim, E., Mark, D. K., Choi, S. & Painter, O. A superconducting quantum simulator based on a photonic-bandgap metamaterial. *Science* **379**, 278–283 (2023).
142. González-Tudela, A., Huidobro, P. A., Martín-Moreno, L., Tejedor, C. & García-Vidal, F. J. Theory of strong coupling between quantum emitters and propagating surface plasmons. *Phys. Rev. Lett.* **110**, 126801 (2013).

143. Garcia-Vidal, F. J., Ciuti, C. & Ebbesen, T. W. Manipulating matter by strong coupling to vacuum fields. *Science* <https://doi.org/10.1126/science.abd0336> (2021).
144. Flick, J., Rivera, N. & Narang, P. Strong light–matter coupling in quantum chemistry and quantum photonics. *Nanophotonics* **7**, 1479–1501 (2018).
145. Orgiu, E. et al. Conductivity in organic semiconductors hybridized with the vacuum field. *Nat. Mater.* **14**, 1123–1129 (2015).
146. Balasubrahmaniam, M. et al. From enhanced diffusion to ultrafast ballistic motion of hybrid light–matter excitations. *Nat. Mater.* **22**, 338–344 (2023).
147. Feist, J., Galego, J. & Garcia-Vidal, F. J. Polaritonic chemistry with organic molecules. *ACS Photonics* **5**, 205–216 (2018).
148. Curtis, J. B., Raines, Z. M., Allocca, A. A., Hafezi, M. & Galitski, V. M. Cavity quantum Eliashberg enhancement of superconductivity. *Phys. Rev. Lett.* **122**, 167002 (2019).
149. Thomas, A. et al. Large enhancement of ferromagnetism under a collective strong coupling of YBCO nanoparticles. *Nano Lett.* **21**, 4365–4370 (2021).
150. Ashida, Y. et al. Quantum electrodynamic control of matter: cavity-enhanced ferroelectric phase transition. *Phys. Rev. X* **10**, 041027 (2020).
151. Dicke, R. H. Coherence in spontaneous radiation processes. *Phys. Rev.* **93**, 99 (1954).
152. Gonzalez-Tudela, A., Laussy, F., Tejedor, C., Hartmann, M. & Del Valle, E. Two-photon spectra of quantum emitters. *New J. Phys.* **15**, 033036 (2013).
153. Pichler, H., Ramos, T., Daley, A. J. & Zoller, P. Quantum optics of chiral spin networks. *Phys. Rev. A* **91**, 42116 (2015).
154. Paulisch, V., Kimble, H. J. & González-Tudela, A. Universal quantum computation in waveguide QED using decoherence free subspaces. *New J. Phys.* **18**, 043041 (2016).
155. Zanner, M. et al. Coherent control of a multi-qubit dark state in waveguide quantum electrodynamics. *Nat. Phys.* **18**, 538–543 (2022).
156. González-Tudela, A., Paulisch, V., Chang, D. E., Kimble, H. J. & Cirac, J. I. Deterministic generation of arbitrary photonic states assisted by dissipation. *Phys. Rev. Lett.* **115**, 163603 (2015).
157. González-Tudela, A., Paulisch, V., Kimble, H. J. & Cirac, J. I. Efficient multiphoton generation in waveguide quantum electrodynamics. *Phys. Rev. Lett.* **118**, 213601 (2017).
158. Stannigel, K., Rabl, P. & Zoller, P. Driven-dissipative preparation of entangled states in cascaded quantum-optical networks. *New J. Phys.* **14**, 063014 (2012).
159. Metelmann, A. & Clerk, A. A. Quantum-limited amplification via reservoir engineering. *Phys. Rev. Lett.* **112**, 133904 (2014).
160. Ramos, T., Pichler, H., Daley, A. J. & Zoller, P. Quantum spin dimers from chiral dissipation in cold-atom chains. *Phys. Rev. Lett.* **113**, 237203 (2014).
161. Ramos, T., Vermersch, B., Hauke, P., Pichler, H. & Zoller, P. Non-Markovian dynamics in chiral quantum networks with spins and photons. *Phys. Rev. A* **93**, 62104 (2016).
162. Liedl, C., Pucher, S., Tebbenjohanns, F., Schneeweiss, P. & Rauschenbeutel, A. Collective radiation of a cascaded quantum system: from timed Dicke states to inverted ensembles. *Phys. Rev. Lett.* **13**, 163602 (2023).
163. Liedl, C. et al. Observation of superradiant bursts in waveguide QED. Preprint at <https://arxiv.org/abs/2211.08940v1> (2022).
164. Evans, R. E. et al. Photon-mediated interactions between quantum emitters in a diamond nanocavity. *Science* **362**, 662–665 (2018).
165. Tiranov, A. et al. Collective super- and subradiant dynamics between distant optical quantum emitters. *Science* **379**, 389–393 (2023).
166. Asenjo-Garcia, A., Moreno-Cardoner, M., Albrecht, A., Kimble, H. J. & Chang, D. E. Exponential improvement in photon storage fidelities using subradiance and ‘selective radiance’ in atomic arrays. *Phys. Rev. X* **7**, 031024 (2017).
167. González-Tudela, A. & Porras, D. Mesoscopic entanglement induced by spontaneous emission in solid-state quantum optics. *Phys. Rev. Lett.* **110**, 080502 (2013).
168. Ask, A. & Johansson, G. Non-Markovian steady states of a driven two-level system. *Phys. Rev. Lett.* **128**, 083603 (2022).
169. Forn-Díaz, P., Lamata, L., Rico, E., Kono, J. & Solano, E. Ultrastrong coupling regimes of light–matter interaction. *Rev. Mod. Phys.* **91**, 025005 (2019).
170. Kockum, A. F., Miranowicz, A., De Liberato, S., Savasta, S. & Nori, F. Ultrastrong coupling between light and matter. *Nat. Rev. Phys.* **1**, 19 (2019).
171. Sanchez-Burillo, E., Zueco, D., Garcia-Ripoll, J. J. & Martin-Moreno, L. Scattering in the ultrastrong regime: nonlinear optics with one photon. *Phys. Rev. Lett.* **113**, 263604 (2014).
172. Schiró, M., Boryduh, M., Ztop, B. & Türeci, H. E. Phase transition of light in cavity QED lattices. *Phys. Rev. Lett.* **109**, 053601 (2012).
173. Kurcz, A., Bermudez, A. & García-Ripoll, J. J. Hybrid quantum magnetism in circuit QED: from spin-photon waves to many-body spectroscopy. *Phys. Rev. Lett.* **112**, 180405 (2014).
174. Román-Roche, J., Sánchez-Burillo, E. & Zueco, D. Bound states in ultrastrong waveguide QED. *Phys. Rev. A* **102**, 023702 (2020).
175. Rivera, N. & Kaminer, I. Light–matter interactions with photonic quasiparticles. *Nat. Rev. Phys.* **2**, 538–561 (2020).
176. Muñoz-Matutano, G. et al. Emergence of quantum correlations from interacting fibre-cavity polaritons. *Nat. Mater.* **18**, 213–218 (2019).
177. Delteil, A. et al. Towards polariton blockade of confined exciton-polaritons. *Nat. Mater.* **18**, 219–222 (2019).
178. Blanco-Redondo, A., Bell, B., Oren, D., Eggleton, B. J. & Segev, M. Topological protection of biphoton states. *Science* **362**, 568–571 (2018).
179. Blanco-Redondo, A. Topological nanophotonics: toward robust quantum circuits. *Proc. IEEE* **108**, 837–849 (2020).
180. Tschernig, K. et al. Topological protection versus degree of entanglement of two-photon light in photonic topological insulators. *Nat. Commun.* **12**, 1974 (2021).
181. Heuck, M., Jacobs, K. & Englund, D. R. Controlled-phase gate using dynamically coupled cavities and optical nonlinearities. *Phys. Rev. Lett.* **124**, 160501 (2020).
182. Tomm, N. et al. Photon bound state dynamics from a single artificial atom. *Nat. Phys.* **19**, 857–862 (2023).
183. Jeannic, H. L. et al. Dynamical photon–photon interaction mediated by a quantum emitter. *Nat. Phys.* **18**, 1191–1195 (2022).

## Acknowledgements

A.G.-T., J.J.G.-R. and F.J.G.-V acknowledge support from the Proyecto Sinérgico CAM 2020 Y2020/TCS-6545 (NanoQuCo-CM). A.G.-T. and J.J.G.-R. acknowledge support from the CSIC Interdisciplinary Thematic Platform (PTI) Quantum Technologies (PTI-QTEP+) and from Spanish projects PID2021-127968NB-I00. A.G.-T. also acknowledges the project TED2021-130552B-C22 funded by MCIN/AEI/10.13039/501100011033/FEDER UE and MCIN/AEI/10.13039/501100011033, respectively, and the support from a 2022 Leonardo Grant for Researchers and Cultural Creators, BBVA. A.R. acknowledges support by the Deutsche Forschungsgemeinschaft (DFG, German Research Foundation) via the project RE 3967/1 and by the German Federal Ministry of Education and Research (BMBF) via the grant agreements no. 13N15907 and 16KISQ046. F.J.G.-V. acknowledges financial support by the Spanish Ministry for Science and Innovation-Agencia Estatal de Investigación (AEI) through grants PID2021-125894NB-I00 and CEX2018-000805-M and by the Comunidad de Madrid and the Spanish State through the Recovery, Transformation, and Resilience Plan (“MATERIALES DISRUPTIVOS BIDIMENSIONALES (2D)” (MAD2D-CM)-UAM7), and the European Union through the Next Generation EU funds.

## Author contributions

The authors contributed equally to all aspects of the article.

## Competing interests

The authors declare no competing interests.

## Additional information

**Peer review information** *Nature Reviews Physics* thanks Salvatore Savasta and the other, anonymous, reviewer(s) for their contribution to the peer review of this work.

**Publisher’s note** Springer Nature remains neutral with regard to jurisdictional claims in published maps and institutional affiliations.

Springer Nature or its licensor (e.g. a society or other partner) holds exclusive rights to this article under a publishing agreement with the author(s) or other rightsholder(s); author self-archiving of the accepted manuscript version of this article is solely governed by the terms of such publishing agreement and applicable law.

© Springer Nature Limited 2024